INTERNATIONAL JOURNAL FOR NUMERICAL METHODS IN FLUIDS
Int. J. Numer. Meth. Fluids **31**: 787–800 (1999)

NUMERICAL SIMULATION OF INCOMPRESSIBLE FLOW DRIVEN BY DENSITY VARIATIONS DURING PHASE CHANGE[1]

E. MCBRIDE[a,*], J.C. HEINRICH[a] AND D.R. POIRIER[b]

[a] *Department of Aerospace and Mechanical Engineering, The University of Arizona, Tucson, AZ 85721, USA*
[b] *Department of Materials Science and Engineering, The University of Arizona, Tucson, AZ 85721, USA*

SUMMARY

A change in density during the solidification of alloys can be an important driving force for convection, especially at reduced levels of gravity. A model is presented that accounts for shrinkage during the directional solidification of dendritic binary alloys under the assumption that the densities of the liquid and solid phases are different but constant. This leads to a non-homogeneous mass conservation equation, which is numerically treated in a finite element formulation with a variable penalty coefficient that can resolve the velocity field correctly in the all-liquid region and in the mushy zone. The stability of the flow when shrinkage interacts with buoyancy flows at low gravity is examined. Copyright © 1999 John Wiley & Sons, Ltd.

KEY WORDS: incompressible flow; phase change; density variations; low gravity

1. INTRODUCTION

The densities of materials in their solid and liquid states are normally different. The change in volume associated with the change in density is usually referred to as shrinkage and may be positive if the solid has a higher density or negative if the solid is less dense than the liquid. During solidification, the difference between densities requires the melt to move toward the solidifying front when the shrinkage is positive or to move away from it when negative; either way, flow is induced in the melt. Even though the magnitude of the velocities produced by the shrinkage is small, especially in the dendritic or mushy zone, this flow may have a strong impact on the solidified composition and contribute to macrosegregation in the cast alloy.

Numerical studies of shrinkage-induced flows in the mushy zone of directionally solidified binary alloys were first performed in the 1970s and early 1980s [1–3]. These simulations considered flow in the mushy zone only and solved the local solute redistribution equation [4] coupled with Darcy's Law for flow in the porous mushy zone. More recently, models based on mixture theory [5] or volume-averaged equations [6–9] have been used to calculate thermosolutal convection in solidifying binary alloys. These models include the all-solid and all-liquid regions, as well as the mushy zone, and were the first ones capable of predicting some severe

* Correspondence to: Department of Aerospace and Mechanical Engineering, The University of Arizona, Tucson, AZ 85721, USA.
[1] This paper was presented at the Tenth International Conference on Finite Elements in Fluids, Tucson, Arizona, 5–8 January 1998.

CCC 0271–2091/99/210787–14$17.50

forms of macrosegregation associated with convection, such as A-segregates and freckles [10,11].

When solidification is effected under the influence of terrestrial gravity, it is generally accepted that the effect of shrinkage-induced flow is not significant. However, Krane and Incropera [12] concluded that, for some alloys and for high solidification rates, the effect of shrinkage is important. Calculations of the solidification of binary alloys including shrinkage have also been reported by Chiang and Tsai [13,14], Xu and Li [15,16], Schneider and Beckermann [17] and Naterer [18]. In these studies, emphasis was placed on assessing the effect of shrinkage-induced flow on macrosegregation under gravity. Also, an effort was made [13,18] to describe the change in the free surface during the solidification process. Calculated pressure in the mushy zone was reported in only one study [15].

In the present work, the effect of density variations are introduced in a vertical solidification model of the binary alloys used by Felicelli *et al.* [11,19], under the restriction that the densities in the liquid and solid phases are different but constant. The focus of the study is the interaction between the shrinkage-induced flow and buoyancy flows at low gravity levels, which is of interest in environments, such as those encountered in the space shuttle or space station.

The appropriate equations are first established, and the numerical method used is then described and validated. Finally, the stability of the flows is examined using a Pb–Sn system under various gravitational conditions.

2. GOVERNING EQUATIONS

The solidification process is examined for a liquid binary alloy contained in a rectangular mold that is cooled at the base at a specified rate. The dendritic zone is modeled as a porous medium, with a non-uniform anisotropic permeability, and is allowed to develop according to the local thermodynamic conditions. The conservation equations of mass, momentum, energy and solute content are solved in two dimensions using the following main assumptions:

1. The liquid is Newtonian and incompressible, and the flow is laminar.
2. Only liquid and solid phases are present; no pores form.
3. There is no solute diffusion in the solid.
4. The densities and specific heat capacities of the solid and liquid are different but constant.
5. All other physical properties are constant and equal in the solid and liquid.
6. The solid is stationary, and the liquid satisfies the Boussinesq approximation.

The mixture density, ρ, in the mushy zone is

$$\rho = \rho_s(1-\phi) + \rho_l\phi, \tag{1}$$

where ϕ is the volume fraction of liquid and ρ_s denotes the density of the solid phase and ρ_l that of the liquid phase. A similar assumption will be made to express the volumetric enthalpy of the mixture, $\overline{\rho H}$, where H denotes the intensive enthalpy in J kg^{-1},

$$\overline{\rho H} = \rho_s H_s(1-\phi) + \rho_l H_l \phi, \tag{2}$$

where the subscripts s and l correspond to the solid and liquid phases respectively. It is also assumed that, in the mushy zone, the enthalpies H_l and H_s are linear functions of temperature, so their difference can be written in the form

$$H_l - H_s = L + (c_{p_l} - c_{p_s})(T - T_H), \tag{3}$$

where T is temperature, c_{p_l} and c_{p_s} are the (constant) specific heat capacities in the liquid and solid respectively, and L is the latent heat at the reference temperature T_H.

The governing equations are obtained using volume averaging, following the work of Ganesan and Poirier [20]. In non-dimensional form, these are as follows:

Continuity:

$$\nabla \cdot \mathbf{u} = \beta \frac{\partial \phi}{\partial t}. \tag{4}$$

Momentum:

$$\phi \frac{\partial}{\partial t}\left(\frac{u_i}{\phi}\right) + \phi \frac{\partial p}{\partial x_i} - \frac{1}{Re} \nabla^2 u_i + \frac{\phi}{Re(Da)_{x_i}} u_i$$
$$= -\mathbf{u} \cdot \nabla\left(\frac{u_i}{\phi}\right) + \frac{\beta}{3Re} \frac{\partial^2 \phi}{\partial x_i \, \partial t} + n_i \phi \left[\frac{Ra_T}{Re^2 Pr} T + \frac{Ra_s}{Re^2 Sc}(c_l - 1)\right]. \tag{5}$$

Energy:

$$[\phi + \gamma(1 - \phi)] \frac{\partial T}{\partial t} - \frac{1}{PrRe} \nabla^2 T$$
$$= -\mathbf{u} \cdot \nabla T - \beta \frac{\partial \phi}{\partial t} T - \left[(1 + \beta)\hat{L} + (1 + \beta - \gamma)(T - \hat{T}_H) \frac{\partial \phi}{\partial t}\right]. \tag{6}$$

Mixture solute concentration:

$$\frac{\partial \overline{\rho c}}{\partial t} = -\frac{\rho_l}{\rho_0}\left[\mathbf{u} \cdot \nabla c_l - \frac{1}{ReSc} \nabla \cdot \phi \nabla c_l + \beta \frac{\partial \phi}{\partial t} c_l\right]. \tag{7}$$

In these equations, u_i denotes the velocity component in the co-ordinate direction x_i, t is time, p is the pressure, n_i is the direction cosines of the gravitational acceleration vector, $\overline{\rho c}$ is the average product of density ρ and the total solute concentration c, and ρ_0 is the reference density. The parameters are:

1. The shrinkage, β: $\beta = (\rho_s - \rho_l)/\rho_l$.
2. The Reynolds number, Re: $Re = VH/\nu_0$.
3. The Darcy coefficients, Da_{x_i}: $Da_{x_i} = K_{x_i}/H^2$.
4. The thermal Rayleigh number, Ra_T: $Ra_T = (\beta_T g G H^4)/(\nu_0 D_T)$.
5. The Prandtl number, Pr: $Pr = \nu_0/D_T$.
6. The solutal Rayleigh number, Ra_s: $Ra_s = (\beta_s g c_0 H^3)/(\nu_0 D_s)$.
7. The Schmidt number, Sc: $Sc = \nu_0/D_s$.
8. The ratio of heat capacities, γ: $\gamma = (\rho_s c_{p_s})/(\rho_l c_{p_l})$.
9. The non-dimensional latent heat, $\hat{L}$: $\hat{L} = L/(c_{p_l} GH)$.
10. The non-dimensional reference temperature, $\hat{T}_H$: $\hat{T}_H = T_H/GH$.

In the above definitions, V and H are respectively the reference velocity and length; ν_0 is the kinematic viscosity; K_{x_i} is the permeability in the direction x_i; which is assumed to be a principal direction; β_T and β_s are the thermal and solutal expansion coefficients; D_T and D_s are the thermal and solutal diffusion coefficients; g is the magnitude of the gravitational acceleration; G is the reference thermal gradient; and c_0 is the reference solute concentration. The temperature is non-dimensionalized using GH as the scale, the reference time is H/V, and the reference pressure is $\rho_0 V^2$. The reference length, H, is chosen to be of the same order as the

primary dendrite arm spacing, and the characteristic velocity is selected as the ratio of an imposed cooling rate (given in the section on numerical simulations) to the initial temperature gradient when gravity is small. For values of g close to terrestrial gravity, the velocity scale is set to $\sqrt{g\beta_T GH^2}$, which is related to the buoyancy.

In the Boussinesq approximation, the density is assumed to be a linear function of temperature and solute concentration,

$$\rho = \rho_l[1 + \beta_T(T - T_0) + \beta_c(c_l - c_0)], \tag{8}$$

where T_0 is the reference temperature and ρ_0 must be the density of the liquid phase at T_0, c_0. In the absence of solute diffusion in the solid, the average solute concentration in the solid, c_s, is given by

$$c_s = \frac{1}{1-\phi}\int_{\phi}^{1} kc_l \, d\phi, \tag{9}$$

where k is the equilibrium partition ratio.

Table I. Physical properties of the Pb–Sn mixture

Property	Reference
Reference temperature (taken as the liquidus temperature of the alloy): $T_0 = 546.5$ K	[26]
Equilibrium partition ratio: $k = 0.31$	[26]
Melting point of lead: $T_M = 600$ K	[26]
Slope of liquidus line: $m = -2.33$ K (wt.%)$^{-1}$	[26]
Liquid density: $\rho_l = 8800$ kg m^{-3}	[27]
Solid density: $\rho_s = 9700$ kg m^{-3}	[27]
Thermal expansion coefficient: $\beta_T = 1.2 \times 10^{-4}$ K^{-1}	[27]
Solutal expansion coefficient: $\beta_c = 5.15 \times 10^{-3}$ (wt.%)$^{-1}$	[27]
Kinematic viscosity: $\nu_0 = 2.47 \times 10^{-7}$ m^2 s^{-1}	[28]
Latent heat: $L = 37.6$ kJ kg^{-1} K^{-1}	[29]
Liquid heat capacity: $c_{p_l} = 0.19$ kJ kg^{-1} K^{-1}	[29]
Solid heat capacity: $c_{p_s} = 0.16$ kJ g^{-1} K^{-1}	[29]
Thermal conductivity: $\kappa = 0.0182$ kW m^{-1} K^{-1}	[30]
Thermal diffusivity: $D_T = 1.1 \times 10^{-5}$ m^2 s^{-1}	[28–30]
Solutal diffusivity: $D_s = 3 \times 10^{-9}$ m^2 s^{-1}	—
Permeability in the x_1-direction (transverse to dendrite growth) in m^2: $K_{x_1} = \begin{cases} 1.09 \times 10^{-3}\phi^{3.32} d_1^2 & \phi < 0.65 \\ 4.04 \times 10^{-6}\left[\dfrac{\phi}{1-\phi}\right]^{6.7336} d_1^2 & 0.65 \le \phi \le 0.75 \\ \left[-6.49 \times 10^{-2} + 5.43 \times 10^{-2}\left[\dfrac{\phi}{1-\phi}\right]^{0.25}\right] d_1^2 & 0.75 \le \phi \le 1 \end{cases}$	[23,25]
Permeability in the x_2-direction (parallel to dendrite growth) in m^2: $K_{x_2} = \begin{cases} 3.75 \times 10^{-4}\phi^2 d_1^2 & \phi < 0.65 \\ 2.05 \times 10^{-7}\left[\dfrac{\phi}{1-\phi}\right]^{10.739} d_1^2 & 0.65 \le \phi \le 0.75 \\ 0.074[\log(1-\phi)^{-1} - 1.49 + 2(1-\phi) - 0.5(1-\phi)^2] d_1^2 & 0.75 \le \phi \le 1 \end{cases}$	[23,25]

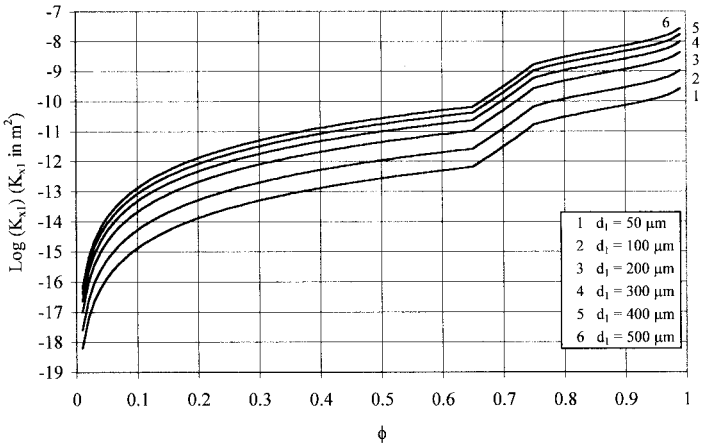

Figure 1. Permeabilities perpendicular to the primary dendrite arm spacing, d_1, as a function of the volume fraction of liquid, ϕ.

Finally, in dendritic freezing processes of alloys, the composition of the dendritic liquid at a given temperature is essentially uniform and the local solid–liquid interface is very close to equilibrium. Therefore, the composition of the interdendritic liquid is given by the liquidus line in the phase diagram, which is assumed to have a constant slope, m. Then, we have

$$c_l = \begin{cases} c & \text{if } \phi = 1 \\ \dfrac{T - T_M}{m} & \text{if } \phi < 1 \end{cases}, \tag{10}$$

where T_M is the melting temperature of the solvent. The concentrations of solute in the solid and liquid, c_s and c_l, are related to the total concentration through the expression

$$\overline{\rho c} = \rho_l c_l \phi + \rho_s c_s (1 - \phi). \tag{11}$$

Because the interest is in vertical directional solidification, it can be assumed that the principal directions of the permeability tensor coincide with the axial system describing the rectangular container. If this is not the case, Equation (5) should be modified to account for the local direction of dendritic growth, which requires a local transformation of the permeability tensor. Details of this procedure are given by Sinha *et al.* [21].

3. FINITE ELEMENT METHOD

The weighted residual form of Equations (4)–(7) is discretized using bilinear isoparametric elements to obtain the velocity, temperature and total solute concentration. The remaining variables, c_s, c_l and ϕ, are calculated at the nodes using Equations (9)–(11) respectively. They are then interpolated for use in the conservation and momentum equations using bilinear elements. The algorithm uses a Petrov–Galerkin formulation for stabilization and the penalty

method to impose incompressibility. Most of the details have already been published in References [19,22] and are not repeated here. However, use of the penalty method to impose incompressibility when the continuity equation is not homogeneous needs to be justified. This is done by first assuming that Equations (4) and (5) have been discretized using a mixed formulation consisting of a bilinear velocity and constant element pressure at the element level. This leads to a discrete system of equations of the form

$$\begin{bmatrix} \mathbf{M} & \mathbf{0} \\ \mathbf{0} & 0 \end{bmatrix} \begin{bmatrix} \dot{\mathbf{u}} \\ \dot{p} \end{bmatrix} + \begin{bmatrix} \mathbf{B} & -\mathbf{C} \\ \mathbf{C}^T & 0 \end{bmatrix} \begin{bmatrix} \mathbf{u} \\ p \end{bmatrix} = \begin{bmatrix} \mathbf{F} \\ G \end{bmatrix}, \tag{12}$$

where the 8×8 matrix $\mathbf{B}$ contains the contribution of the diffusion and Darcy terms only. The non-linear and buoyancy terms are placed in the vector $\mathbf{F}$. The element G contains the contribution of the right-hand-side term in the continuity equation.

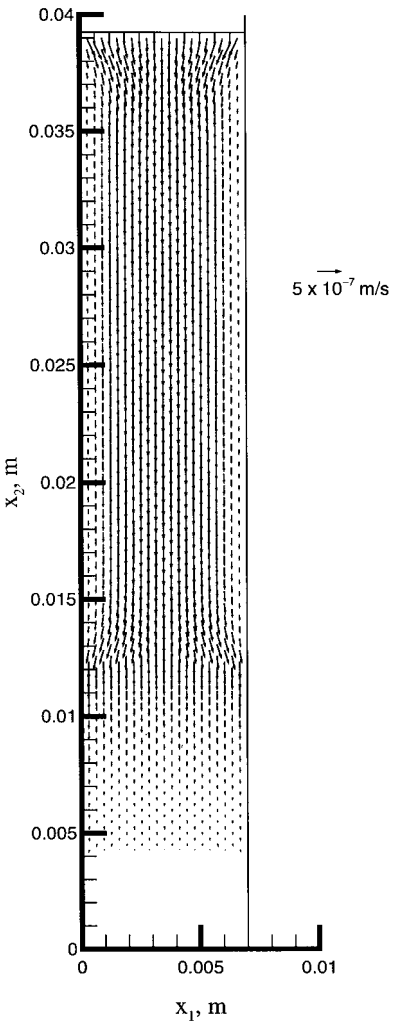

Figure 2. Results for solidification at zero gravity after 4000 s, with $d_1 = \mu$m.

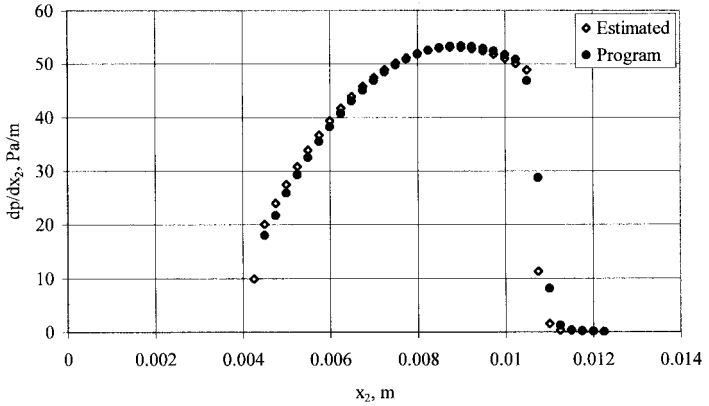

Figure 3. Vertical pressure gradient in the mushy zone as calculated and estimated from Darcy's Law. Same conditions as Figure 2.

In the second square matrix of Equation (12), the zero diagonal element is approximated by $1/\lambda$, where λ is the penalty parameter, which is positive and large. Multiplying and manipulating this modified expression, one obtains the equations

$$\mathbf{M}\dot{\mathbf{u}} + (\mathbf{B} + \lambda \mathbf{C}\mathbf{C}^T)\mathbf{u} = \mathbf{F} + \lambda \mathbf{C}\mathbf{G} \tag{13}$$

and

$$p = -\lambda(\mathbf{C}^T\mathbf{u} - \mathbf{G}). \tag{14}$$

The last equation gives the constant dynamic pressure over the element and is equivalent to defining it by the relation

$$p - p_s = -\lambda\left(\nabla\cdot\mathbf{u} - \beta\frac{\partial\phi}{\partial t}\right), \tag{15}$$

where p is the total pressure and p_s is the static pressure. In the present implementation, Equation (13) is constructed using bilinear shape functions only, with a one-point reduced integration quadrature used to integrate all penalized terms.

Because the mushy zone is modeled as a porous medium, the Darcy term becomes important in the momentum equation when $1 < \phi < 0.6$ and dominant when $\phi < 0.6$. This poses a numerical difficulty because the permeability varies by many orders of magnitude as ϕ goes from one to zero. The permeabilities used in this work are based on References [23–25] and are given in Table I. Figure 1 shows the permeability perpendicular to the primary dendrite arm spacing as a function of the volume fraction of liquid. To accommodate this wide range of variability in the permeability, a variable penalty parameter, λ, is used. This λ is defined as a step function that depends on the volume fraction of liquid, with value $\lambda = 10^9$ if $\phi > 0.9$ and $\lambda = 10^{15}$ if $\phi < 0.9$. The effectiveness of this modified penalty method in calculating the flow in these two-phase situations is shown in the following section.

Two different strategies have been used to account for the fact that the volume of liquid in the container is changing. The first assumes that the top is an open boundary through which liquid at the initial melt composition, c_0, is allowed to enter to compensate for the volume change due to solidification. This is a good approximation, as long as thermosolutal convection in the fluid does not reach the top. The second method assumes that the top free surface

always remains planar and moves downward as a rigid lid. At each time step, the change in volume, Δ, is calculated from

$$\Delta = \int_{\Omega} \beta \frac{\partial \phi}{\partial t} \, d\Omega, \tag{16}$$

where Ω is the domain. Knowing Δ, one can calculate the velocity of the free surface, and the distance it moves is adjusted accordingly. This approach is no longer valid once the mushy zone reaches the free surface. However, the objective is not to study the last stage of the solidification, and the calculations are not carried out for times long enough for the mushy zone to reach the top surface.

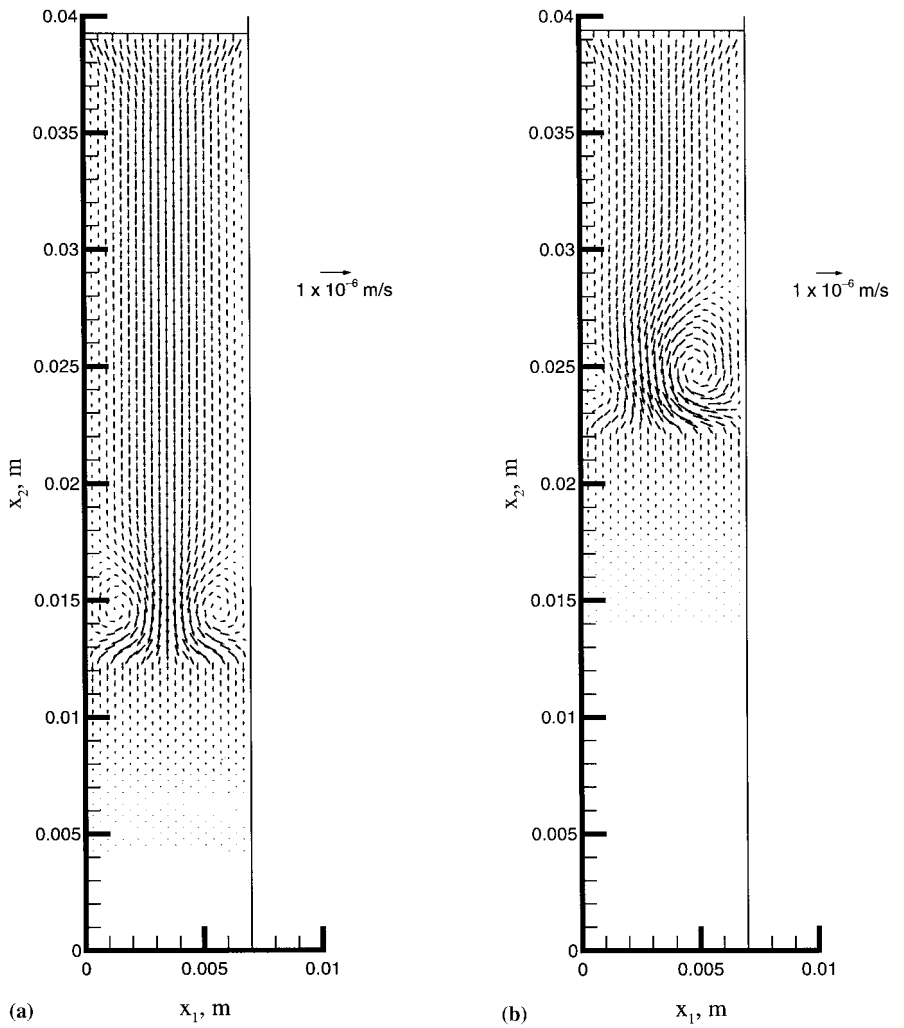

Figure 4. Detail of flow instability ahead of the mushy zone at $|g_2| = 2 \times 10^{-4} g_0$: (a) unperturbed flow at 4000 s; (b) perturbed flow at 7000 s.

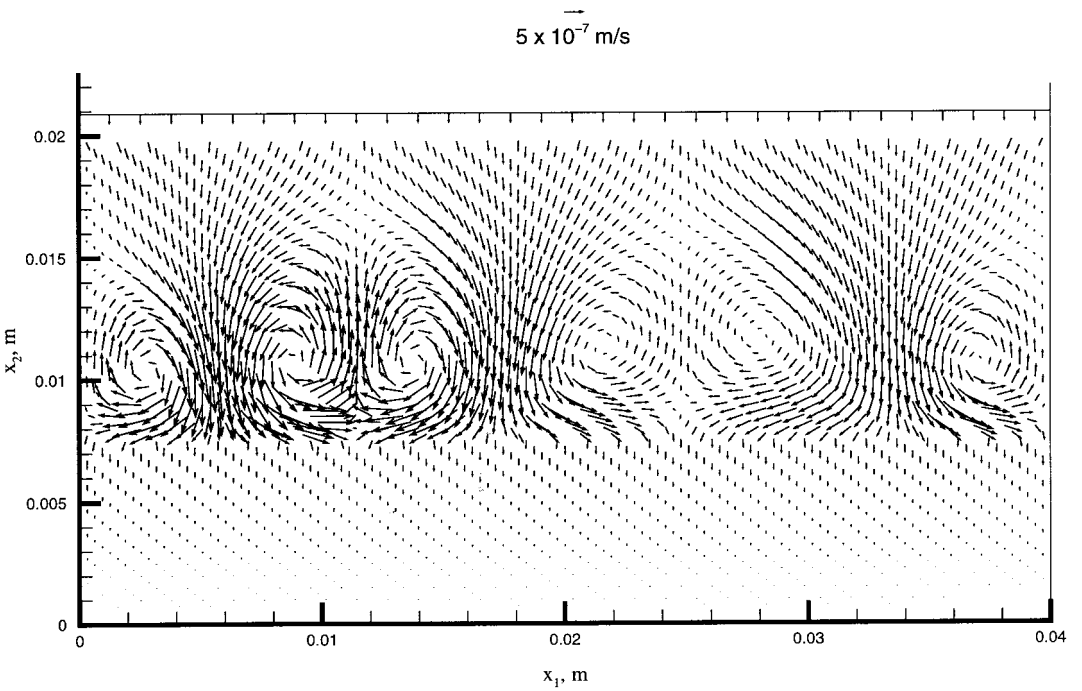

Figure 5. Flow instability at $|g_2| = 2 \times 10^{-4} g_0$ in a container 4 cm wide. Except for width, same conditions as Figure 2.

4. NUMERICAL SIMULATIONS

Two-dimensional simulations of the solidification of a Pb–23wt.%Sn alloy in a rectangular container of dimensions 0.007 m wide by 0.04 m high are considered. Initially, a linear temperature gradient of 100 K m^{-1} is imposed with the temperature at the bottom of the container equal to the freezing temperature of the alloy. The physical properties used in the calculations are given in Table I. No-slip is imposed along the boundaries, and a sliding rigid lid is applied at the top of the container. The side walls are assumed to be adiabatic, and the initial temperature gradient is maintained at the top surface throughout the calculation. Under these conditions, the primary dendrite arm spacing, d_1, is 200 μm, in accordance with Reference [31]. The latent heat is taken at the reference temperature, $T_H = 528$ K. Initially, the melt is at rest, and a constant cooling rate is applied uniformly at the bottom of the container for $t \geq 0$.

In the first calculation, it is assumed that there is no gravitational field, i.e. $\mathbf{g} = 0$. This case is used to validate the algorithm. The cooling rate applied at the bottom is 0.03333 K s^{-1}, and the flow in the casting is driven entirely by the change in density in the solidifying mushy zone. Figure 2 shows the results after 4000 s of solidification time. The bottom 4 mm are fully solidified, the mushy zone spans the region between 4 and 12.3 mm, and the rest is still all liquid. At the top, we observe that the rigid lid has moved down approximately 0.8 mm due to shrinkage. The uniform velocity of the rigid lid evolves into a fully developed Poiseuille flow within the top 5 mm of the container. The pressure gradient in the overlying liquid in the vertical direction in the fully developed section shows only a 5% difference when compared with the solution for Poiseuille flow using the calculated maximum vertical velocity at the

centerline, which is -3.859×10^{-7} m s^{-1}. When the liquid encounters the top of the mushy zone, it diverges toward the vertical surfaces and reverts back to a uniform vertical velocity at a given x_2 within the mushy zone. Figure 3 shows the vertical pressure gradient in the vertical direction along the centerline in the mushy zone as calculated in the program using the penalty approximation and estimated directly from the Darcy equation

$$\frac{\partial p}{\partial x_2} = \mu K_{x_2}^{-1} u_2, \tag{17}$$

where μ is the viscosity, and the vertical velocity component, u_2, is the calculated velocity. It is observed that the agreement is indeed excellent and that the flow within the mushy zone is dominated by the Darcy term as expected.

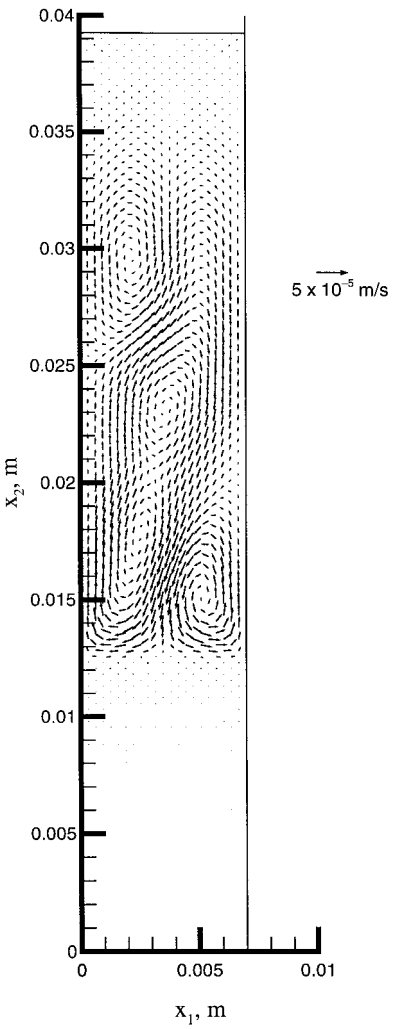

Figure 6. Results showing flow dominated by thermosolutal convection at 4000 s for $|g_2| = 10^{-3} g_0$. Except for gravity level, same conditions as Figure 4(a).

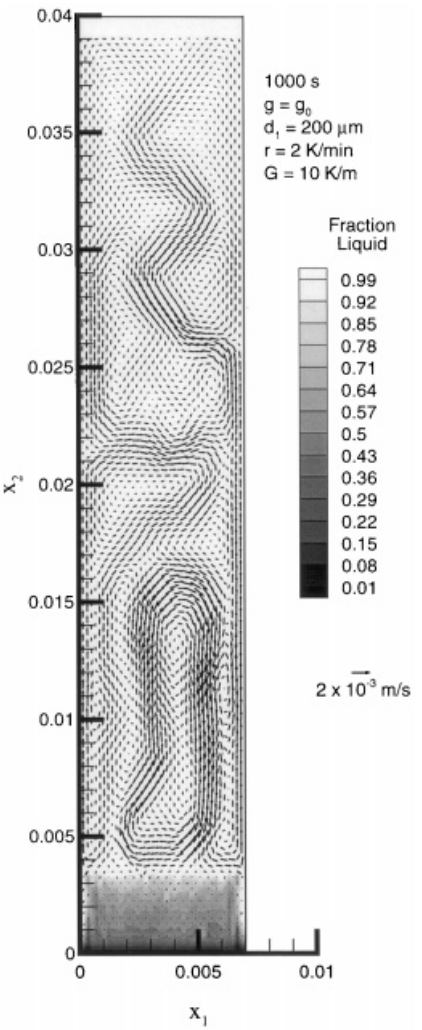

Figure 7. Flow at 1500 s for $|g_2| = g_0$ with strong convection in channels and macrosegregation within the mushy zone.

The gravitational force in the negative vertical direction is now increased. No significant change from the $\mathbf{g} = 0$ case is observed up to about $|g_2| = 10^{-4} g_0$, where $g_0 = 9.8\ \mathrm{m\,s^{-2}}$ is the terrestrial gravity. Figure 4(a) shows results after 4000 s of solidification at $|g_2| = 2 \times 10^{-4} g_0$. Here, it is observed that the interaction of the shrinkage flow with the lighter solute-enriched layer at the top of the mushy zone forms two recirculation cells in the all-liquid flow just above the mushy zone. This flow is itself unstable, and when perturbed, one of the cells becomes dominant, as shown in Figure 4(b) at 7000 s. Calculations on wider geometries show that these cells also exhibit a spatial wavelength in the horizontal direction, which, in the present calculations, appeared to be confined to between 7 and 13 mm. This is shown in Figure 5 for a container 4 cm wide after 2000 s of solidification time for the same conditions discussed above.

Further increase in the gravitational force leads to a regime typical of double-diffusive flows in which the stratification due to solute redistribution leads to circulation cell patterns that

now are significantly stronger. An example of this is given in Figure 6, where results for $|g_2| = 10^{-3} g_0$ at 4000 s show that the flow due to shrinkage is almost negligible, as compared with the thermsolutal flow. Figure 7 shows the flow field for $|g_2| = g_0$ at 1000 s. The effect of gravity becomes overwhelming in Figure 7, which shows strong channels developing in the mushy zone and very strong thermosolutal convection with velocities two orders of magnitude larger than in Figure 6. A further effect of the strong convection in the liquid is depicted in Figure 8(a), which shows how the isotherms are affected by convection. The calculated pressure for this last case at $|g_2| = g_0$ is shown in Figure 8(b), where the effect of the strong convection in the mushy zone is evident. The solute concentration in the channels reaches as much as 30wt% and will result in defects in the cast known as freckles.

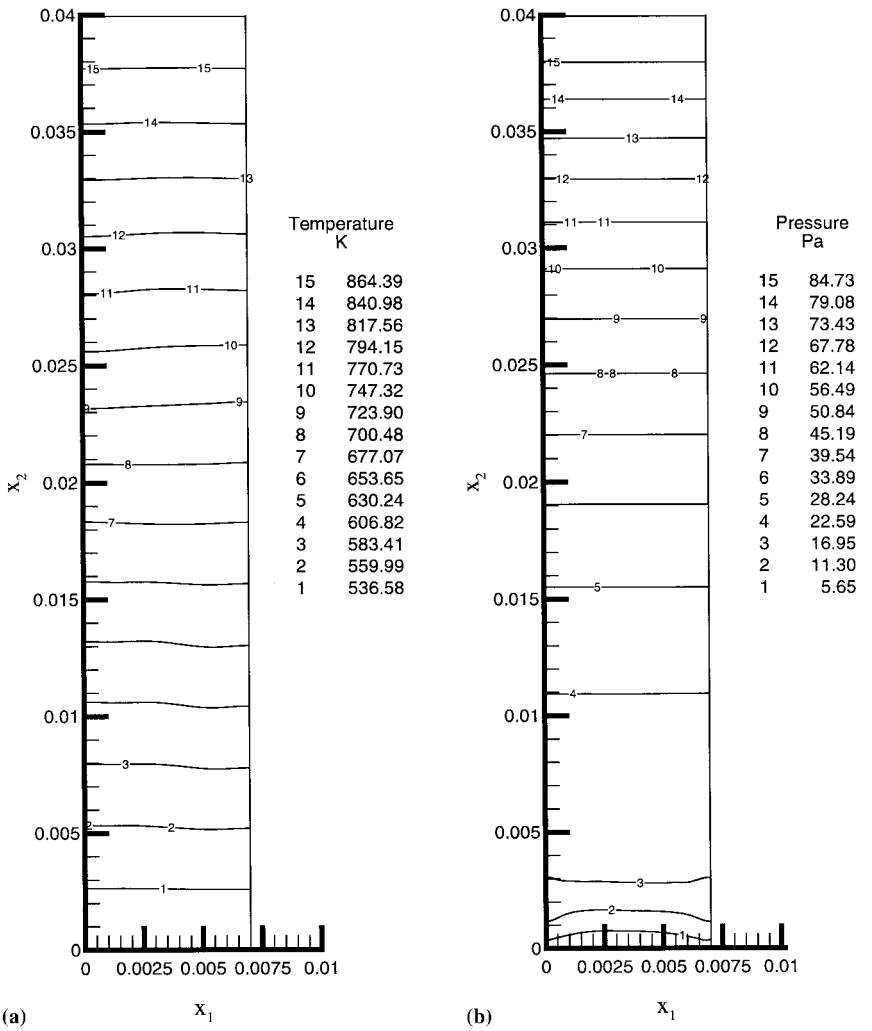

Figure 8. Calculated temperature and pressure at 1500 s for $|g_2| = g_0$ showing the disturbances due to the channels in the mushy zone: (a) temperature; (b) pressure. Same conditions as Figure 7.

5. CONCLUSIONS

A mathematical model of the solidification of binary alloys that includes shrinkage induced by a change of density due to a phase change has been developed under the simplifying assumption that the densities in the fluid and solid phases are different, but constant. The finite element model of Felicelli *et al.* [19] was extended to this case by means of a generalized penalty function approximation using a variable penalty parameter applied to the non-homogeneous continuity equation that results. The model has been applied to solidification of binary alloys under zero and reduced gravity conditions. The results indicate that the shrinkage flow is stable, but when it interacts with buoyancy at $|g_2| \approx 2 \times 10^{-4} g_0$ or greater levels of gravity, instabilities develop that induce flow in the melts. The results also show that, for slow rates of solidification, the effect of shrinkage on the overall flow pattern is negligible under terrestrial gravity conditions.

ACKNOWLEDGMENTS

This work has been supported by the National Aeronautics and Space Administration under grant NCC8-96. The authors are grateful to Dr Sergio Felicelli for his help.

REFERENCES

1. R. Mehrabian, M. Keane and M.C. Flemings, 'Interdendritic fluid flow and macrosegregation; influence of gravity', *Metall. Trans.*, **1**, 1209–1220 (1970).
2. T. Fujii, D.R. Poirier and M.C. Flemings, 'Macrosegregation in a multicomponent low alloy steel', *Metall. Trans. B*, **10**, 331–338 (1979).
3. A.L. Maples and D.R. Poirier, 'Convection in the two-phase zone of solidifying alloys', *Metall. Trans. B*, **15**, 163–172 (1984).
4. M.C. Flemings and G.E. Nereo, 'Macrosegregation: part I', *Trans. TMS-AIME*, **239**, 1449–1461 (1967).
5. W.D. Bennon and F.P. Incropera, 'A continuum model for momentum, heat and species transport in binary solid–liquid phase change systems—I. Model formulations', *Int. J. Heat Mass Transf.*, **30**, 2161–2170 (1987).
6. V.R. Voller and C. Prakash, 'A fixed grid numerical modelling methodology for convection–diffusion mushy region phase-change problems', *Int. J. Heat Mass Transf.*, **30**, 1709–1719 (1987).
7. C. Beckerman and R. Viskanta, 'Mathematical modeling of transport phenomena during alloy solidification', *Appl. Mech. Rev.*, **46**, 1–26 (1993).
8. G. Amberg, 'Computation of macrosegregation in an iron–carbon cast', *Int. J. Heat Mass Transf.*, **34**, 217–227 (1991).
9. D.R. Poirier and J.C. Heinrich, 'A continuum model for predicting macrosegregation', *Mater. Charactr.*, **32**, 287–298 (1994).
10. W.D. Bennon and F.P. Incropera, 'A continuum model for momentum, heat and species transport in binary solid–liquid phase change systems, II. Application to solidification in a rectangular cavity', *Int. J. Heat Mass Transf.*, **30**, 2171–2187 (1987).
11. S.D. Felicelli, J.C. Heinrich and D.R. Poirier, 'Simulation of freckles during vertical solidification of binary alloys', *Metall. Trans. B*, **22**, 847–859 (1991).
12. M.J.M. Krane and F.P. Incropera, 'Analysis of the effect of shrinkage on macrosegregation in alloy solidification', *Transport Phenomena in Solidification*, ASME HTD-Vol. 284/AMD-Vol. 182, ASME, New York, 1994, pp., 13–27.
13. K.C. Chiang and H.L. Tsai, 'Shrinkage-induced fluid flow and domain change in two-dimensional alloy solidification', *Int. J. Heat Mass Transf.*, **35**, 1763–1770 (1992).
14. K.C. Chiang and H.L. Tsai, 'Interaction between shrinkage-induced fluid flow and natural convection during alloy solidification', *Int. J. Heat Mass Transf.*, **35**, 1771–1778 (1992).
15. D. Xu and Q. Li, 'Numerical method for solution of strongly coupled binary alloy solidification problems', *Num. Heat Transf. A*, **20**, 181–201 (1991).
16. D. Xu and Q. Li, 'Gravity and solidification—shrinkage-induced liquid flow in a horizontally solidified alloy ingot', *Numer. Heat Transf. A*, **20**, 203–221 (1991).
17. M.C. Schneider and C. Beckermann, 'A numerical study of the combined effects of microsegregation, mushy zone permeability and flow, caused by volume contraction and thermosolutal convection, on macrosegregation and eutectic formation in binary alloy solidification', *Int. J. Heat Mass Transf.*, **38**, 3455–3473 (1995).

18. G.F. Naterer, 'Simultaneous pressure–velocity coupling in the two-phase zone for solidification shrinkage in an open cavity', *Model. Simul. Mater. Sci. Eng.*, **5**, 595–613 (1997).
19. S.D. Felicelli, J.C. Heinrich and D.R. Poirier, 'Numerical model for dendritic solidification of binary alloys', *Numer. Heat Transf. B*, **23**, 461–481 (1993).
20. S. Ganesan and D.R. Poirier, 'Conservation of mass and momentum for the flow of interdendritic liquid during solidification', *Metall. Trans. B*, **21**, 163–181 (1990).
21. S.K. Sinha, T. Sundararajan and V.K. Garg, 'A variable property analysis of alloy solidification using the anisotropic porous medium approach', *Int. J. Heat Mass Transf.*, **35**, 2865–2877 (1992).
22. S.D. Felicelli, J.C. Heinrich and D.R. Poirier, 'Finite element analysis of directional solidification of multicomponent alloys', *Int. J. Numer. Methods Fluids*, **27**, 207–227 (1998).
23. D.R. Poirier, 'Permeability of flow of interdendritic liquid in columnar–dendritic alloys', *Metall. Trans. B*, **18**, 245–255 (1987).
24. M.S. Bhat, D.R. Poirier and J.C. Heinrich, 'Permeability of cross flow through columnar dendritic alloys', *Metall. Trans. B*, **26**, 1049–1056 (1995).
25. S. Ganesan, C.L. Chan and D.R. Poirier, 'Permeability for flow parallel to primary dendrities', *Mater. Sci. Eng. A*, **151**, 97–105 (1992).
26. T. Lyman (ed.), *Metals Handbook*, 8th edn., vol. 8, American Society of Metals, Metals Park, OH, 1973.
27. D.R. Poirier, 'Densities of Pb–Sn alloys during solidification', *Metall. Trans. A.*, **19**, 2349–2354 (1988).
28. H.R. Thresh and A.F. Crawley, 'Viscosities of lead, tin and Pb–Sn alloys', *Metall. Trans.*, **1**, 1531–1535 (1970).
29. D.R. Poirier and P.J. Nandapurkar, 'Enthalpies of a binary alloy during solidification', *Metall. Trans. A*, **19**, 3057–3061 (1988).
30. D.R. Poirier, P.J. Nandapurkar and S. Ganesan, 'The energy and solute conservation equations for dendritic solidification', *Metall. Trans. B*, **22**, 889–900 (1991).
31. J.T. Mason, J.D. Verhoeven and R. Trivedi, 'Primary dendritic spacing, I. Experimental studies', *J. Cryst. Growth*, **59**, 516–524 (1982).

